GEOPHYSICS, VOL. 58, NO. 4 (APRIL 1993); P. 482–495, 8 FIGS.

Audio-frequency electromagnetic tomography in 2-D

Qiang Zhou*, Alex Becker‡, and H. F. Morrison‡

ABSTRACT

The mathematical formulation of acoustic diffraction tomography is applied to the problem of low frequency, diffusive electromagnetic (EM) fields. EM tomographic inversion, in two-dimensional (2-D) Cartesian geometry, is illustrated for a crosshole source-receiver configuration. The object function of the conductivity distribution is related to the transformed and filtered data by an inverse Fourier transform in the vertical direction and an inverse Laplace transform in the lateral direction. The reconstructed conductivity image is found to be a band-limited version of the actual conductivity distribution. To stabilize the inversion, a regularized least-squares method is used for image reconstruction. As in the seismic case, the inversion quality can be understood by inspecting the wavenumber domain coverage of the object function. Numerical experiments show that the resolution is better in the vertical direction than in the horizontal and it is also a function of source operating frequency. The position and attitude of the target are recovered well.

INTRODUCTION

Tomography is the visual representation or imaging of a given physical property within a region inaccessible to direct view. The term was first used in x-ray studies where the absorption of an x-ray beam passing through a body is proportional to the integral of the density along the path. Integrals along multiple paths can determine the full three-dimensional (3-D) distribution of density within the body. This technique has obvious appeal in geophysics where the goal is to determine the distribution of physical properties in the subsurface. Since high-frequency elastic waves in liquids or solids follow ray theory, tomography was introduced in acoustics and seismology soon after its successes in x-ray analysis. In some materials, high-frequency electromagnetic waves (radar) also satisfy ray theory, and tomography shows some promise in this area (e.g., Deadrick et al., 1982). At low frequencies, however, ray theory becomes inappropriate and diffraction must be taken into account. Diffraction tomography based on the wave equation produces satisfactory images. But low-frequency EM fields in the earth are governed by the diffusion equation, and it is not obvious that traditional tomography is applicable to diffusive fields. However, early work in this area by Howard et al. (1983), referred to by them as "wave diffusion tomography," did demonstrate that the subsurface eddy currents could be mapped.

In this paper, we briefly review the concepts of ray and diffraction tomography and then extend these ideas to crosshole imaging of electrical conductivity with audio-frequency EM fields. Our approach to the inversion of crosshole EM data, which we have termed diffusion tomography, is tested on data generated with a forward modeling code for targets in a conductive background.

RAY AND DIFFRACTION TOMOGRAPHY

In ray tomography, parallel straight line integrals of a 2-D function define the projection of that function in a given direction. The Fourier transform of the resulting projection gives the values of the transform of the function itself along a straight line in 2-D transform space. Thus, each projection provides a slice of the transform of the function. If enough projections are used, the transform of the object can be determined and the inverse transform will yield the object itself. This relation, which has come to be called the Fourier projection-slice theorem appears to have been popularized by Bracewell (1956). It came into widespread use in medical imaging with x-rays and was subsequently introduced in sonic and seismic imaging. Excellent reviews of this topic are found in Mersereau and Oppenheim (1974) and Kak and Slaney (1987). These authors also describe practical details of implementing reconstruction algorithms based on the projection-slice theorem.

Manuscript received by the Editor September 3, 1991; revised manuscript received August 10, 1992.
*Formerly University of California at Berkeley, Berkeley, CA 94720; presently Atlas Wireline Services, P.O. Box 1407, Houston, TX 77251.
‡University of California at Berkeley, Berkeley, CA 94720.
© 1993 Society of Exploration Geophysicists. All rights reserved.

When the wavelength of the incident wavefield is about the same as the scale of the spatial variation of the object function, diffraction effects invalidate any straight line propagation assumptions and a full wave solution is required. It is convenient to represent the scattered or diffracted fields by an integral equation, which describes a superposition of point scatterers energized by the incident field. For an incident uniform plane wave and weak scattering, Wolf (1969) showed that a relation similar to the projection-slice theorem exists between the 2-D transform of the diffracted field and the 3-D Fourier transform of the scatterer. Pan and Kak (1983) presented a general tutorial paper on diffraction tomography, and Devaney (1984) summarized seismic and high-frequency electromagnetic applications.

The diffraction theorem, which Pan and Kak (1983) have called the Fourier diffraction-projection theorem, states: When a 2-D object is illuminated with a plane wave, the Fourier transform of the forward scattered fields measured on a line perpendicular to the direction of propagation of the incident field gives the value of the 2-D Fourier transform of the object along a circular arc in transform space. These arcs are tangential to the Fourier slice lines at zero wavenumber and degenerate into these lines in the short wavelength, nondiffracting limit. This theorem applies only when the Born approximation is satisfied in the integral formulation of the scattered fields. The Fourier diffraction-projection theorem is very useful for describing the seismic reconstruction of objects from measurements made between wells, between a well and the surface (VSP), and from conventional surface reflection surveys. Each of these source-receiver configurations results in a distinctive coverage of the 2-D transform of the object. The accuracy of the reconstruction of the object itself is related to the wavenumber coverage. A thorough analysis of this concept is presented by Devaney (1984) and Wu and Toksöz (1987). There are many ways to reconstruct the object function in diffraction tomography. Devaney (1984) developed a method he termed back propagation. Slaney and Kak (1985) described interpolation schemes in the wavenumber domain to allow the direct use of the inverse FFT to arrive at the object function.

The mathematical formulation of the scattering problem in the frequency domain is the same for seismic and EM problems. For high-frequency electromagnetic fields in dielectrics, the parallels continue through to the algorithms for actually reconstructing the scatters. But low-frequency EM fields in a conductive medium, where displacement currents are negligible, are governed by a diffusion equation. While the solutions have the same form as wavefields, the wavenumbers are complex and diffusive fields cannot be represented by integrals of uniform plane waves with real angles of incidence. The wavenumber coverage diagrams for explaining the reconstruction accuracy or resolution are useful when both the incident and scattered fields can be represented by superpositions of uniform plane waves propagating with real wavenumbers and at real angles with respect to the source or measuring axes. For the diffusion equation, the wavenumbers are complex and the integral representation requires wavenumbers covering the complex plane. Finally, conductivity contrasts in the ground can be huge, up to several orders of magnitude and so the Born approximation, the basis of the Fourier diffraction-projection theorem, may not be suitable for practical problems. This fact has probably discouraged efforts to extend the treatment of Wu and Toksöz (1987) or Devaney (1984) into the low-frequency diffusion regime.

2-D ELECTROMAGNETIC SCATTERING

We follow the papers by Devaney (1984) and Wu and Toksöz (1987) in choosing a 2-D model for studying the low-frequency diffusive EM fields. In the conceptual model (Figure 1), an infinite line source of current is parallel to the 2-D scatterer and the measurements of the scattered field are taken along a borehole in the plane transverse to the scatterer. The electromagnetic fields can then all be derived from the component of electric field parallel to the source E_y and the governing diffusion equation is simply

$$\nabla^2 E_y + k^2 E_y = 0, \tag{1}$$

where $k^2 = -i\omega\mu\sigma$, σ is the electric conductivity, μ is the magnetic permeability, and a time dependence of $e^{i\omega t}$ is used. In the acoustic case the corresponding equation for the pressure u is

$$\nabla^2 u + k^2 u = 0, \tag{2}$$

where $k^2 = \omega^2/c^2$ and c is the sound velocity.

Mathematically, the solutions to both equations have the same form. Since diffraction tomography starts from equation (2), we can simply follow that development while keeping in mind that k is now complex rather than real. The first step is to cast the problem in terms of an integral equation. The electric field at an observation coordinate $\mathbf{r}_g$ for a given source at $\mathbf{r}_s$ may be written as the sum of a

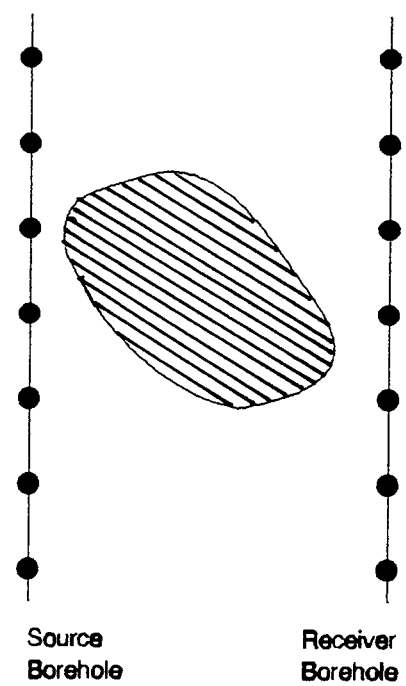

FIG. 1. An illustration of the 2-D model.

primary or incident field plus a secondary or scattered field due to the object.

$$E_y(\mathbf{r}_g, \mathbf{r}_s) = E_y^p(\mathbf{r}_g, \mathbf{r}_s) + E_y^s(\mathbf{r}_g, \mathbf{r}_s), \tag{3}$$

where E_y^p is the primary field from the source and E_y^s is the secondary field produced by the scattering currents. The subscript y will be deleted in the subsequent development. A solution to the general scattering problem shown in Figure 1 may be found by replacing the object with a volume distribution of scattering currents and expressing the resulting fields by an integration of the appropriate Green's function and the scattering currents (Ward and Hohmann, 1988).

$$\begin{aligned} E^s(\mathbf{r}_g, \mathbf{r}_s) &= -i\omega\mu \int\int J^s(\mathbf{r}, \mathbf{r}_s)G(\mathbf{r}_g, \mathbf{r})\, dx\, dz \\ &= -\int\int k_0^2 O(\mathbf{r})E(\mathbf{r}, \mathbf{r}_s)G(\mathbf{r}_g, \mathbf{r})\, dx\, dz. \end{aligned} \tag{4}$$

The target is assumed to be localized such that the integration is over the cross-section between the boreholes. The constant k_0^2 is the background wavenumber ($k_0^2 = -i\omega\mu\sigma_0$, where σ_0 is the background conductivity). The scattering currents $J^s(\mathbf{r}, \mathbf{r}_s)$ is the product of the total electric field and the difference in conductivity between the scatterer and the background.

$$J^s(\mathbf{r}, \mathbf{r}_s) = [\sigma(\mathbf{r}) - \sigma_0]E(\mathbf{r}, \mathbf{r}_s). \tag{5}$$

The Green's function is given by

$$G(\mathbf{r}_g, \mathbf{r}) = -\frac{i}{4} H_0^{(2)}(k_0|\mathbf{r}_g - \mathbf{r}|). \tag{6}$$

This Green's function is slightly different from the definition in Ward and Hohmann (1988, p. 179) but its form is identical to that in Wu and Toksöz (1987). The object function $O(\mathbf{r})$ is defined as

$$O(\mathbf{r}) = 1 - \sigma(\mathbf{r})/\sigma_0 = 1 - k^2(\mathbf{r})/k_0^2. \tag{7}$$

Equation (4) is a Fredholm integral equation of the second kind, and it relates the object function $O(\mathbf{r})$ to the scattered electric field. In forward modeling, the object profile $O(\mathbf{r})$ is known everywhere and the solution for the scattered fields is straightforward in principle. Computationally however, its solution may be difficult for an arbitrary conductivity distribution because the problem size may be impractically large for current computers. In the inverse problem to solve for $O(\mathbf{r})$, the field values of E^s or E are only known over a limited set of space points which usually lie outside the object volume of interest, and one has to solve for both the object function and the electric field inside the volume. This inverse problem is not linear. One way of simplifying it is to use the weak-scattering, or Born approximation, in which the total electric field inside the integral is replaced by the primary field. Then, the only unknown is the object function $O(\mathbf{r})$ or the medium property $\sigma(\mathbf{r})$. Although there are severe limitations to such an approximation in EM application, the insights provided offer an understanding of the EM inverse problem.

THE BORN APPROXIMATION SOLUTION

Under the Born approximation,

$$E(\mathbf{r}, \mathbf{r}_s) \approx E^p(\mathbf{r}, \mathbf{r}_s). \tag{8}$$

For a unit (1 ampere) source strength,

$$E^p(\mathbf{r}, \mathbf{r}_s) = -i\omega\mu G(\mathbf{r}, \mathbf{r}_s). \tag{9}$$

Equation (4) now becomes

$$E^s(\mathbf{r}_g, \mathbf{r}_s) = i\omega\mu \int\int k_0^2 O(\mathbf{r})G(\mathbf{r}, \mathbf{r}_s)G(\mathbf{r}_g, \mathbf{r})\, dx\, dz. \tag{10}$$

According to Gradshteyn and Ryzhik (1980, formula 6.616.4), the Fourier transform of the Hankel function in the z-direction is

$$\int_{-\infty}^{\infty} H_0^{(2)}(k_0|\mathbf{r} - \mathbf{r}'|)e^{-ik_z z}\, dz = \frac{2}{\gamma} e^{-i\gamma(x - x') - ik_z z'}, \tag{11}$$

where $\gamma^2 = k_0^2 - k_z^2$. For a crosshole geometry, if one takes Fourier transforms of equation (10) along the source and receiver arrays, i.e., with respect to z_g and z_s, respectively,

$$\begin{aligned} E^s(x_g, k_g; x_s, k_s) &= \frac{-i\omega\mu k_0^2}{4\gamma_g\gamma_s} e^{(i\gamma_s x_s - i\gamma_g x_g)} \\ &\cdot \int\int O(\mathbf{r})e^{-i(\gamma_s - \gamma_g)x - i(k_s + k_g)z}\, dx\, dz, \end{aligned} \tag{12}$$

where k_s and k_g are the Fourier domain wavenumbers corresponding to z_s and z_g and

$$\gamma_s^2 = k_0^2 - k_s^2, \tag{13}$$

$$\gamma_g^2 = k_0^2 - k_g^2. \tag{14}$$

Variables x_s and x_g are the horizontal coordinates of the vertical source and receiver arrays.

These steps are similar to those taken in acoustic diffraction tomography. While the acoustic case is based on the real wavenumber k_0, the electromagnetic problem requires its complex equivalent so that further parallelism is inappropriate. We introduce the following substitutions,

$$k_s + k_g = k_z, \tag{15}$$

$$i(\gamma_s - \gamma_g) = s_x. \tag{16}$$

Equation (12) now takes on the form,

$$\begin{aligned} E^s(x_g, k_g; x_s, k_s) \frac{4\gamma_g\gamma_s}{-i\omega\mu k_0^2} e^{(-i\gamma_s x_s + i\gamma_g x_g)} \\ = \int\int O(\mathbf{r})e^{-s_x x - ik_z z}\, dx\, dz. \end{aligned} \tag{17}$$

Define a Laplace transform pair as follows:

$$f(s) = \int_0^{\infty} f(x)e^{-sx}\, dx,$$

$$f(x) = \frac{1}{2\pi i} \int_{\tau - i\infty}^{\tau + i\infty} f(s)e^{sx}\, ds, \tag{18}$$

where $f(x)$ is zero for $x < 0$, and $\int_0^\infty |f(x)| e^{-\tau x}\, dx$ is finite for $\tau > \tau_0 \geq 0$. Since the inhomogeneities are contained within a finite volume, one can always shift the origin to make $O(\mathbf{r}) = 0$ for $x < 0$ and also to ensure that $\int_0^\infty |O(x, z)|\, dx$ with $\tau_0 = 0$ remains finite. In principle, $O(\mathbf{r})$ can be found by taking the inverse Fourier transform in k_z and inverse Laplace transform in s_x of the left-hand side of equation (17).

$$O(\mathbf{r}) = \frac{1}{(2\pi)^2 i} \int\int \left[E^s(x_g, k_g; x_s, k_s) \cdot \frac{4\gamma_g \gamma_s}{-i\omega\mu k_0^2} e^{-i\gamma_s x_s + i\gamma_g x_g} \right] e^{s_x x + i k_z z}\, ds_x\, dk_z, \tag{19}$$

where γ_s, γ_g, k_s, and k_g can all be expressed in k_z and s_x.

Another way of arriving at the linearized solution for the object function is to use the Rytov approximation in the original integral equation as described for seismic applications in Devaney (1981), Cheng (1984), Oristaglio (1985). A comparison of these two approximations for the electromagnetic inverse problem is presented by Zhou (1989).

NUMERICAL CONSTRUCTION OF 2-D TOMOGRAPHIC IMAGE

In principle, the inverse Laplace and inverse Fourier transform representation of the object function in equation (19) provides a direct way of evaluating the object function. The problem, however, is that the numerical inverse Laplace transform is ill-posed and unstable even for noise free but band-limited data (Bertero, 1982). To solve for the conductivity structure and to reduce the uncertainty in the solution, one needs to smooth and constrain the solution (Bertero et al., 1983) as required in regularization theory. For targets more conductive than the background, we can incorporate such a constraint by discretizing the integral equation given in equation (17) and solving the resulting constrained least-squares problem using quadratic programming.

A least-squares scheme can easily be developed for either the wavenumber domain equation (17) or space domain equation (10) to solve for the object function. The wavenumber representation, however, preserves some numerical advantages and also allows a simple extension of the algorithm to problems with cylindrical symmetry. Integral equation (17) is discretized on a rectangular grid over the area of interest,

$$E^s(x_g, k_g; x_s, k_s) \frac{4\gamma_g \gamma_s}{-i\omega\mu k_0^2} = \sum_{j=1}^{N} O_j \cdot \int_j\int e^{-i[\gamma_s(x - x_s) + k_s z]} e^{-i[\gamma_g(x_g - x) + k_g z]}\, dx\, dz, \tag{20}$$

where the integration is carried out on each of the N pixels. Element O_j is the average of the object function over the jth pixel. This equation can be written as

$$p_i = \sum_{j=1}^{N} s_{ij} O_j, \tag{21}$$

where p_i is the filtered response or the left-hand side of equation (20), i is the ith wavenumber combination of (k_g, k_s), and s_{ij} is the weight for jth pixel.

$$s_{ij} = \int_j\int e^{-i[\gamma_s(x - x_s) + k_s z]} e^{-i[\gamma_g(x_g - x) + k_g z]}\, dx\, dz. \tag{22}$$

If we have M wavenumber combinations, for an N pixel image, a linear system of equations can be obtained.

$$S_1 O = P_1, \tag{23}$$

where $S_1 = [s_{ij}]_{N \times M}$ is an $N \times M$ full matrix related to the geometry and wavenumbers, $O = [O_1, O_2, \ldots, O_N]^T$ is an N element solution vector, and $P_1 = [p_1, p_2, \ldots, p_M]^T$ is an M element vector of the filtered measurements. Equation (23) is a system of equations with complex coefficients and is reorganized into real equations. Let

$$S = \begin{bmatrix} Re(S_1) \\ Im(S_1) \end{bmatrix}, \qquad P = \begin{bmatrix} Re(P_1) \\ Im(P_1) \end{bmatrix}. \tag{24}$$

Equation (23) becomes

$$SO = P. \tag{25}$$

This linear system of equations relates the electric conductivity anomaly, or the object function, with the measured secondary field.

The Fourier transform is a plane wave decomposition. The exponential terms in s_{ij} are plane waves with $e^{-i[\gamma_s(x-x_s)+k_s z]}$ corresponding to an incident wave to the jth pixel and $e^{-i[\gamma_g(x_g-x)+k_g z]}$ corresponding to the scattered wave from the same pixel. These plane waves differ in incident or scattering angles and attenuation. The summation from $j = 1$ to N combines the contributions from every pixel. The linear system of equations in (25) is similar to that used in acoustic ray tomography (Peterson, 1986). However, in ray tomography, only the pixels along a straight or curved raypath contribute to the measured response. For the EM problem, a full matrix is required to describe the process. Conventional methods [such as the algebraic reconstruction technique (ART) algorithm discussed in Huesman et al., 1977] do not work because the matrix equation is unstable. Thus, constraints and smoothing are introduced to ensure the stability of the solution. To solve equation (25), we minimize the ℓ_2 norm of the misfit of a particular solution O', or minimize

$$s(O') = \|SO' - P\|^2 \tag{26}$$

subject to the constraints

$$L_i \leq O'_i \leq U_i; \qquad i = 1, 2, \ldots, N. \tag{27}$$

L_i and U_i are the lower and upper bounds, respectively. For example, if we set $L_i = -\infty$ and $U_i = 0$ everywhere, we limit the object function to be smaller than zero. In other words, one then only considers the case where the conductivity of the target is greater than the reference background.

The constraints in equation (27) stabilize the solution and, more importantly, greatly enhance the target resolution (Stark, 1987).

Equation (26) can be rewritten

$$s(O') = O'^T S^T S O' - 2P^T S^T O' + P^T P, \qquad (28)$$

which is in a quadratic form. Equations (27) and (28) together constitute a quadratic programming problem (Gill et al., 1981). Several mathematical program libraries, such as HARWELL (Hopper, 1979), contain subroutines for its solution. To further stabilize the inverse problem, proper smoothing is also incorporated into the constrained least-squares inversion (Zhou, 1989).

NUMERICAL EXAMPLES

Characteristics of the inversion and the validity of the weak-scattering approximation for a crosshole experiment are illustrated with some numerical examples. The effects of individual parameters such as operating frequency, target conductance and target geometry are analyzed to illustrate the resolution inherent in the diffusion response. The exact forward solutions are calculated with a 2-D modeling code as described in Zhou (1989).

The crosshole experiment is simulated with a borehole separation of 100 m and a source or receiver array length of 310 m with 32 source and 32 receiver positions of equal separation in each array. This crosshole configuration results in 1024 different source-receiver combinations. An image area of 100 m by 160 m with 10 m × 10 m pixels is located in the central part of the source and receiver arrays. A 2-D target lies in a homogeneous medium of conductivity 0.01 S/m. Simple single-pixel targets with conductivity twice that of the background are tested first, followed by one or two thin sheet conductors. Each thin sheet target has a thickness-conductivity product of 0.1 S and a width or dip length of 80 m. The object function is constrained to be less than zero. All these parameters will be kept constant unless otherwise noted.

The question of resolution for diffusive electromagnetic fields is addressed using two 10 m × 10 m targets shown in Figures 2 and 3. Vertical resolution as a function of frequency is demonstrated for frequencies of 20, 10, 5, 2.5, and 1.25 kHz which correspond to wavelengths in the background medium of 224, 316, 447, 632, and 894 m, respectively. The target separation is fixed at 50 m. For the vertically separated targets in Figure 2, the estimates of their separation and of the object function are best at 20 kHz. The maximum indicated value of the object function is much lower than its actual value but the total conductance is about correct. As the frequency decreases the targets are seen to be separate down to 1.25 kHz but the apparent separation is less than 50 m and the object function is too small. Nevertheless at this frequency the apparent resolution is about 1/20 of the wavelength.

For the horizontally separated targets shown in Figure 3, the estimate of the separation is also best at 20 kHz, but it is not as good as the estimate of that parameter in the case of vertical target separation. The object function is not well determined and the targets lose their separation below 5 kHz or roughly 1/10 of a wavelength. The vertical position of the targets however, remains well defined. From the above examples, it is clear that for a crosshole source-receiver array the horizontal resolution is related directly to the operating frequency; the higher frequencies give better resolution. For this crosshole source-receiver configuration, better resolution is seen in the vertical than along the horizontal. This phenomenon was also observed by Wu and Xu (1979) in holographic image reconstruction of electromagnetic data collected from physical modeling experiments.

The study of resolution is further illustrated in Figures 4 and 5. Here two rectangular targets are progressively separated by 50 to 20 m in the vertical and horizontal directions, respectively, at a fixed operating frequency of 20 kHz corresponding to a skin depth of 36 m or a wavelength of approximately 224 m in the background medium. At this high frequency, the correct vertical separation is determined up to the point where the objects can no longer be resolved, at a separation of 30 m, or about 1/7 of a wavelength. In the horizontal direction, neither the correct separation nor the ability to resolve the two targets is preserved below a separation of 50 m or one quarter of a wavelength.

The definition of resolution as a function of wavelength and target separation is not straightforward. Vertically separated objects can be resolved (imaged as two separate features) at quite low frequencies yielding an apparent resolution as high as 1/20 of a wavelength. This appears to be somewhat better than the classical wave theory result which indicates that a minimum separation of 1/4 of a wavelength is needed before two point scatterers can be resolved. However, it must be noted that here the resolution is defined by a model of finite rectangular pixels and more importantly under a positivity constraint for the object function.

Another test of this technique is the image reconstruction of the thin sheet model shown in Figures 6 and 7. The thin sheet is infinitely long and has dip angles, β, of 0, 45 and 90 degrees. The target has a thickness-conductivity product of 0.1 S. In general, the target position, dip angle, and dip length are resolved correctly (Figure 6). To reexamine the target resolution in the horizontal and vertical directions, we use the two thin conductors shown in Figure 7. The two targets are parallel to each other and are 40 m apart in the vertical direction. The dip angle varies from 0 to 60 degrees (Figure 7a to 7d). Both the 0 degree and 30 degree cases provide a very good estimate of the thin conductors. As the dip angle increases further to 45 and 60 degrees, the resolution in the horizontally shielded area becomes very poor.

TARGET RESOLUTION AND WAVENUMBER DOMAIN COVERAGE

Two major sources of inaccuracy limit the quality of the reconstructed images in our numerical simulation. One is the limitation of the Born approximation, which might be overcome with a better nonlinear algorithm. The other is due to the source-receiver array configuration and the operating frequency. The explicit representation of the object function by equation (19) provides a way of studying resolution as in diffraction tomography. The wavenumber domain coverage of the object function for the crosshole source-receiver arrangement helps clarify the characteristics demonstrated numerically in the previous section.

According to equation (19), if every point in the wavenumber domain (s_x, k_z) is known, the object function can be determined exactly, and the inversion yields a unique solution. However, this is not possible because, first, the source and receiver positions are discrete and thus can only give discrete samples of k_s and k_g and, through equations (13)–(16), can only give discrete samples of the object function in its transform domain. Secondly, the maximum coverage of the object function in the wavenumber domain is determined by the background wavenumber k_0, which depends on the operating frequency and the background conductivity and by the maximum Fourier domain wavenumbers k_s and k_g. Different source-receiver configurations give distinctive patterns of wavenumber domain coverage and thus control the reconstruction quality.

For a source array length D_s and a constant source interval Δ_s, k_s takes the values given below,

$$k_s = 0,\ \pm 1 \cdot (2\pi/D_s),\ \pm 2 \cdot (2\pi/D_s),\ \ldots,\ \pm\pi/\Delta_s. \tag{29}$$

Similarly, for receiver array length D_g and constant sampling interval Δ_g, k_g takes the following values

$$k_g = 0,\ \pm 1 \cdot (2\pi/D_g),\ \pm 2 \cdot (2\pi/D_g),\ \ldots,\ \pm\pi/\Delta_g. \tag{30}$$

To take advantage of the inverse Fourier transform representation of the object function, k_0 must be greater than $|k_s|$ and $|k_g|$ in the acoustic problem. Because of the introduction of the complex Laplace wavenumber s_x in the EM problem, there is no limit imposed on k_0. From a practical point of

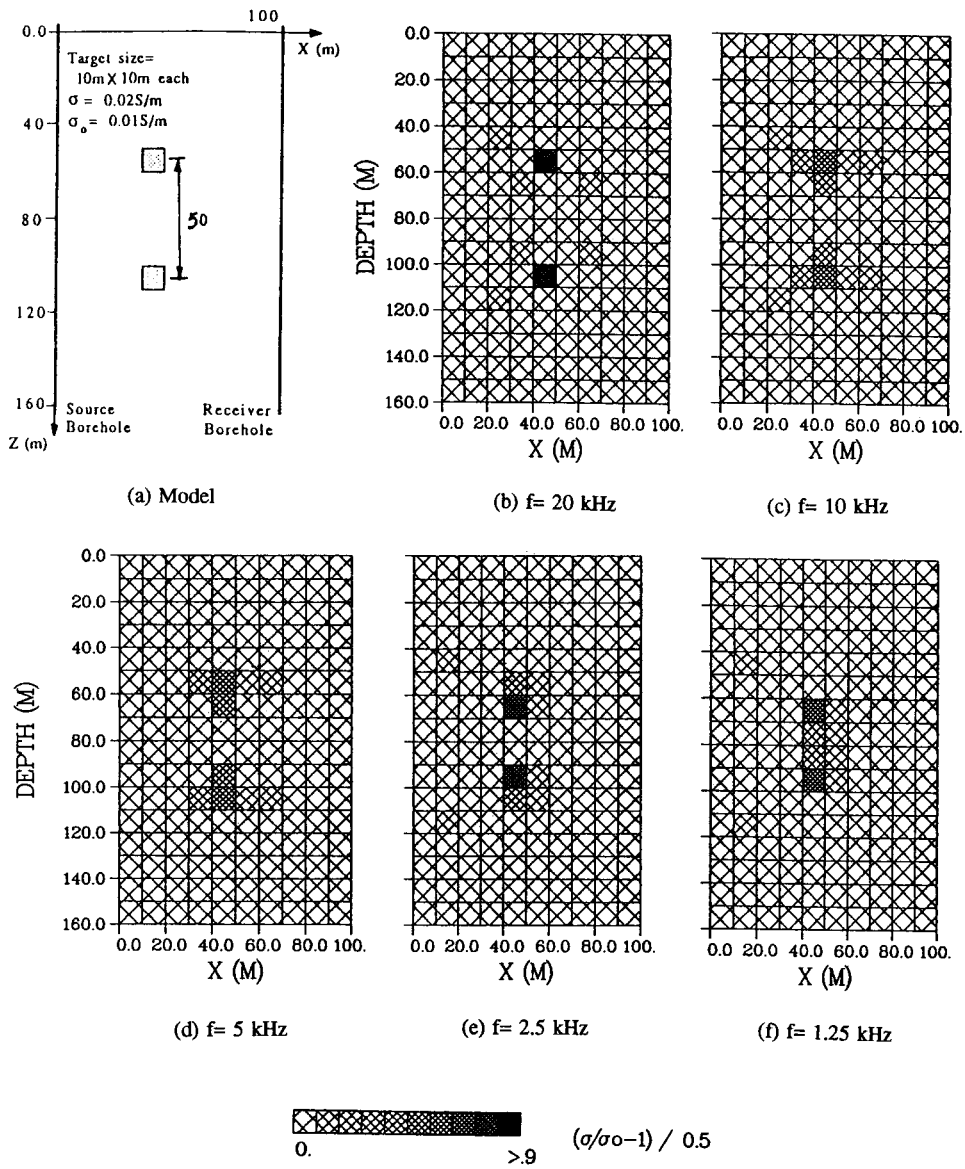

FIG. 2. Images of vertically separated point objects. (a) Model, (b) $f = 20$ kHz, (c) $f = 10$ kHz, (d) $f = 5$ kHz, (e) $f = 2.5$ kHz, (f) $f = 1.25$ kHz.

view $|k_0|$ is much smaller than $|k_g|$ or $|k_s|$ since a large $|k_0|$ implies a severe attenuation of the EM field. The relationship between the given values of (k_s, k_g, k_0) and (k_z, s_x) are provided in equations (13) through (16).

The wavenumber domain coverage for the transmitter-receiver configuration used in the previous models is shown in Figure 8a, where only the positive part of $Re(s_x)$ is shown. It should be noted that the real and imaginary components of s_x are paired and the wavenumber domain coverage is in three dimensions (k_z and the real and imaginary parts of s_x) instead of in two as in the acoustic problem. The coverage in Figure 8b is the 2-D projection on the k_z and $Im(S_x)$ plane. The projection of Figure 8a on the k_z and $Re(S_x)$ plane is shown in Figure 8c. If we take a slice, say along $k_z = \pi/\Delta_s$, of Figure 8a, the resulting relation between $Re(s_x)$ and $Im(s_x)$ is plotted in Figure 8d. The inverse Laplace transform should be carried out along a path from $\tau - i\infty$ to $\tau + i\infty$, while here it is confined to the curved path as in Figure 8d with extremely limited coverage in the direction of imaginary axis. It can be seen on the $(k_z, Im(s_x))$ plane that the coverage in the x-direction is less than one tenth of its extent in the z-direction. Due to the severe attenuation associated with higher operating frequency or background wavenumber, little can be done to increase the lateral or x-direction coverage.

As indicated by Wu and Toksöz (1987) for acoustic diffraction tomography, poor resolution in the lateral or x-direction is expected for this crosshole EM problem because of the poor horizontal wavenumber coverage. Theoretically, in the acoustic situation one can increase the resolution by raising the operating frequency and the sampling density. In the electromagnetic application the image

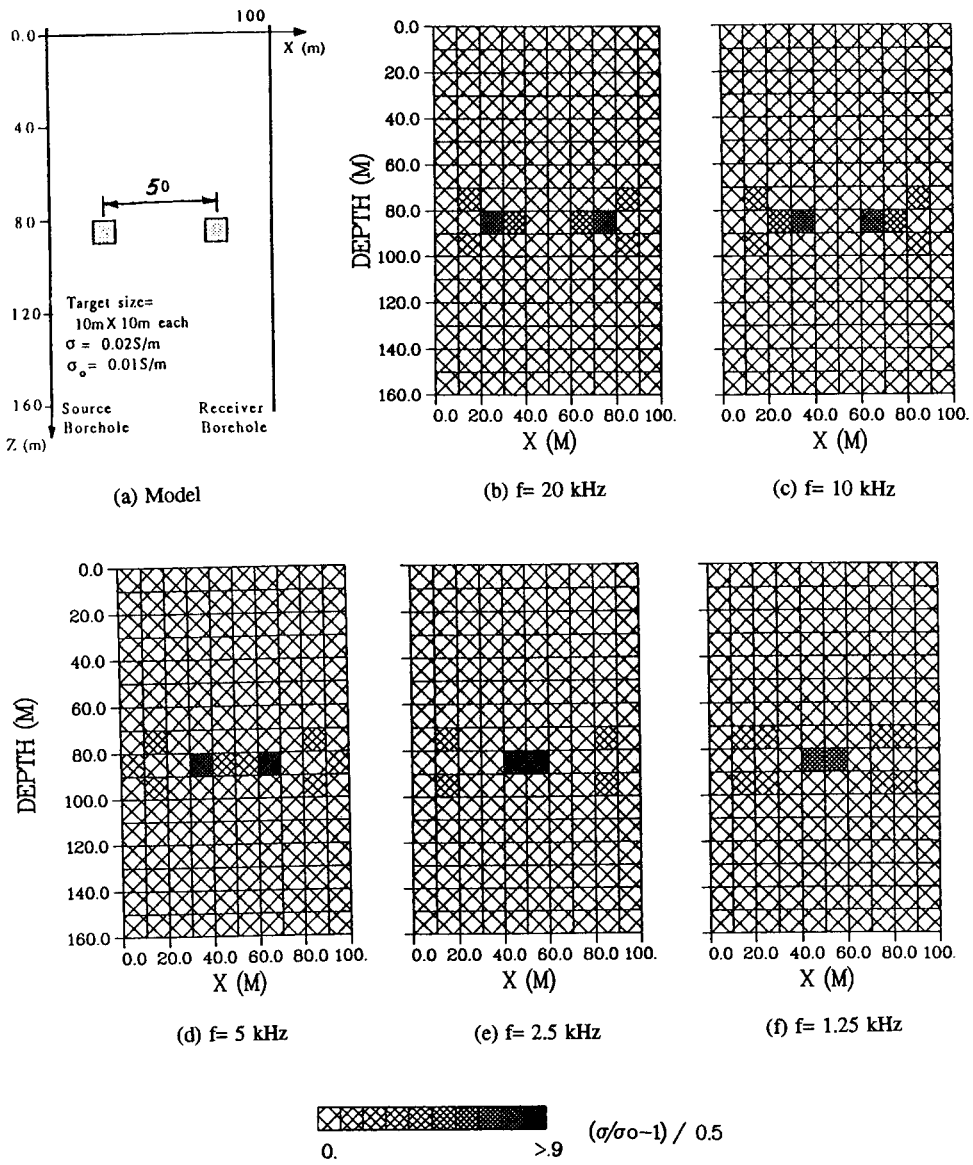

FIG. 3. Images of horizontally separated point objects. (a) Model, (b) f = 20 kHz, (c) f = 10 kHz, (d) f = 5 kHz, (e) f = 2.5 kHz, (f) f = 1.25 kHz.

quality is limited because of severe attenuation at high frequency. Increased sampling density in the crosshole EM case improves the vertical resolution somewhat but provides little help to the horizontal resolution.

SUMMARY

The inversion of 2-D audio-frequency electromagnetics has been investigated by analogy with acoustic diffraction tomography. For a target of low conductivity contrast with the background medium, the Born weak scattering approximation is applied to linearize the problem. For a crosshole source-receiver configuration, the object function or the conductivity distribution can be expressed by an inverse Fourier transform in the vertical direction, and an inverse Laplace transform in the lateral, of the filtered measurements. A regularized least-squares method is actually used in image reconstruction for solution stability. The target resolution is directly related to the source-receiver array arrangement and the source operating frequency. For crosshole source-receiver arrays, the horizontal resolution is much poorer than the vertical, and higher operating frequencies give better image quality.

Because audio-frequency electromagnetic fields are diffusive in an electrically conductive medium, the wavenumber domain coverage in the EM case is 3-D instead of 2-D as in the acoustic problem. Nevertheless coverage diagrams can still be used to analyze the properties of the image reconstruction algorithm. For crosshole source-receiver configuration, the horizontal coverage is much smaller than the vertical coverage, and thus the spatial resolution in the lateral direction is much poorer than that in the vertical. The maximum lateral resolution is related to the source frequency, but because of attenuation arbitrarily high frequencies cannot be used. The spatial features of the target such as

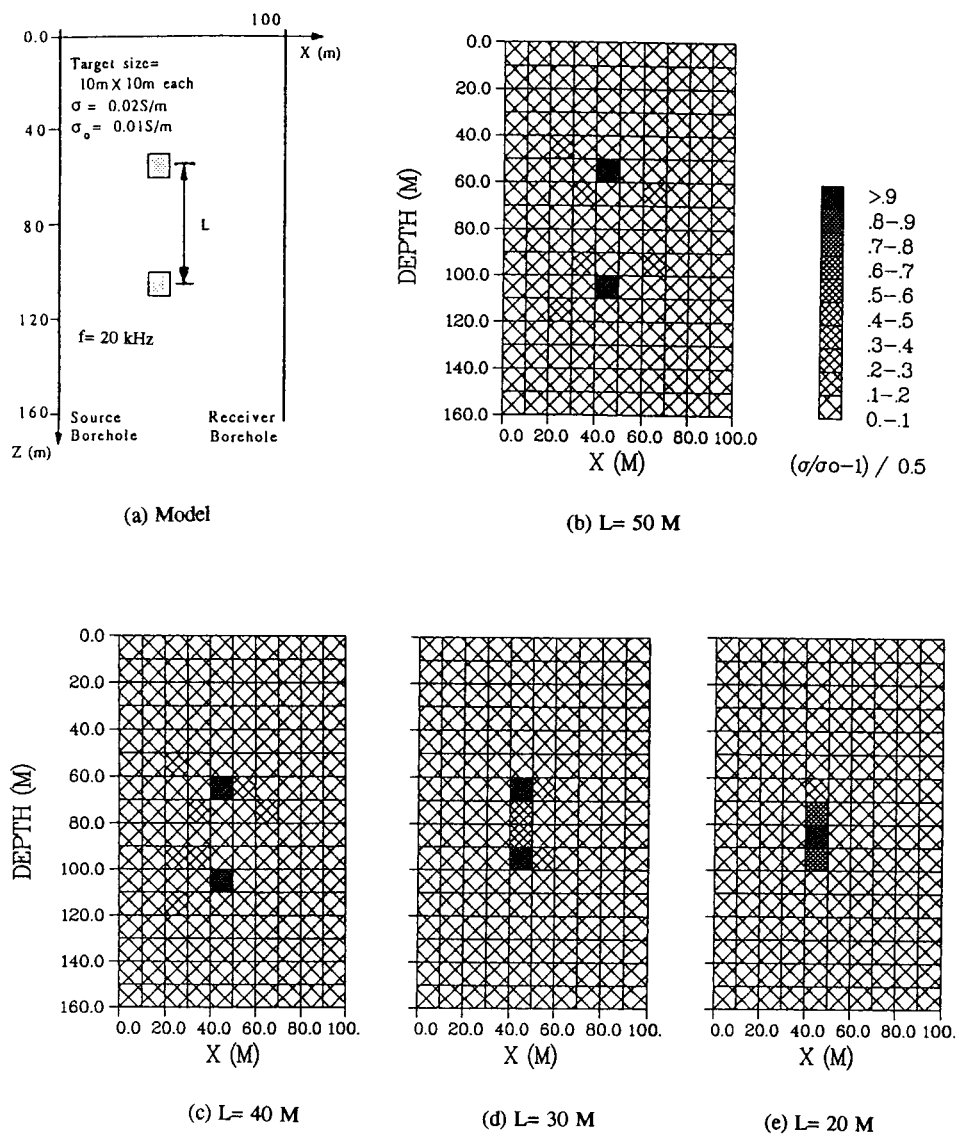

(a) Model (b) L= 50 M (c) L= 40 M (d) L= 30 M (e) L= 20 M

FIG. 4. Images of vertically separated point objects. (a) Model, (b) L = 50 m, (c) L = 40 m, (d) L = 30 m, (e) L = 20 m.

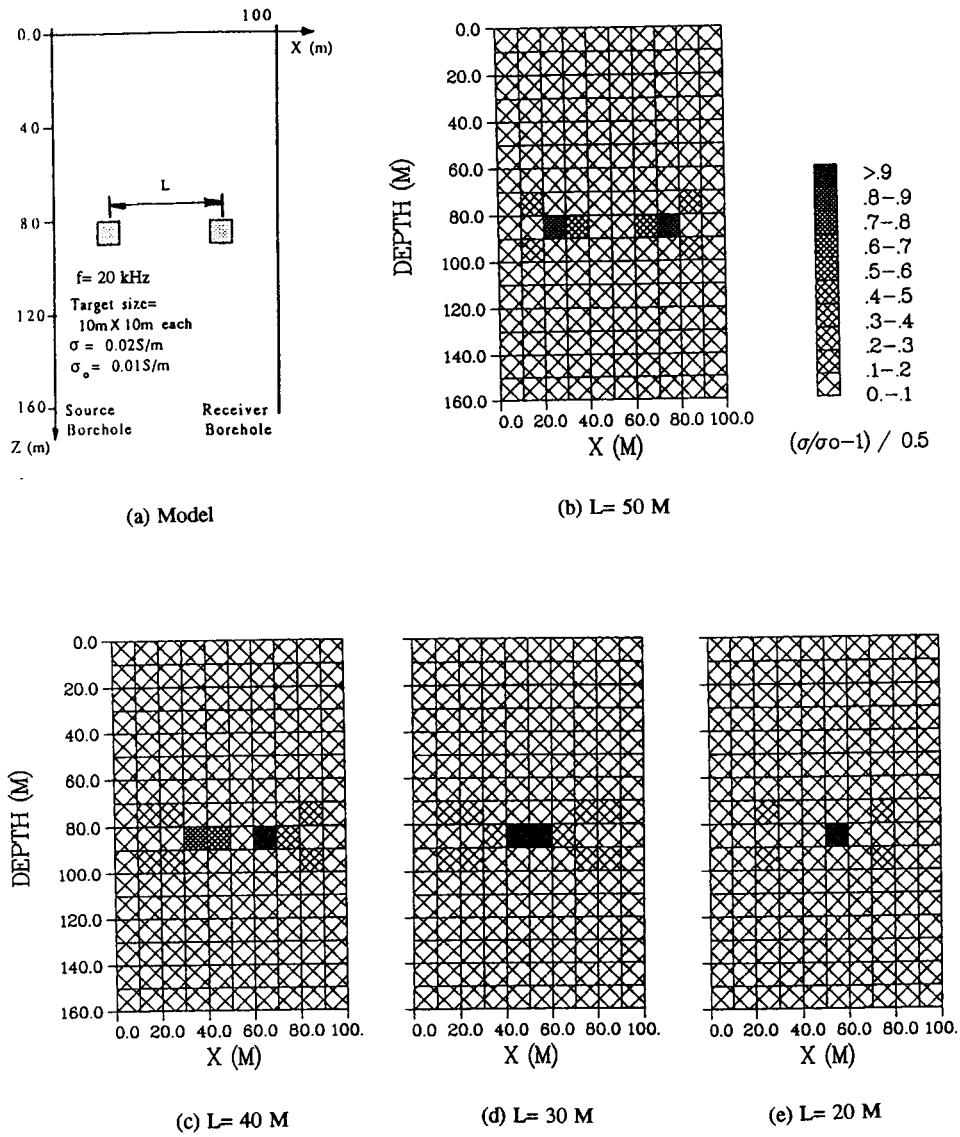

FIG. 5. Images of horizontally separated point objects. (a) Model, (b) L = 50 m, (c) L = 40 m, (d) L = 30 m, (e) L = 20 m.

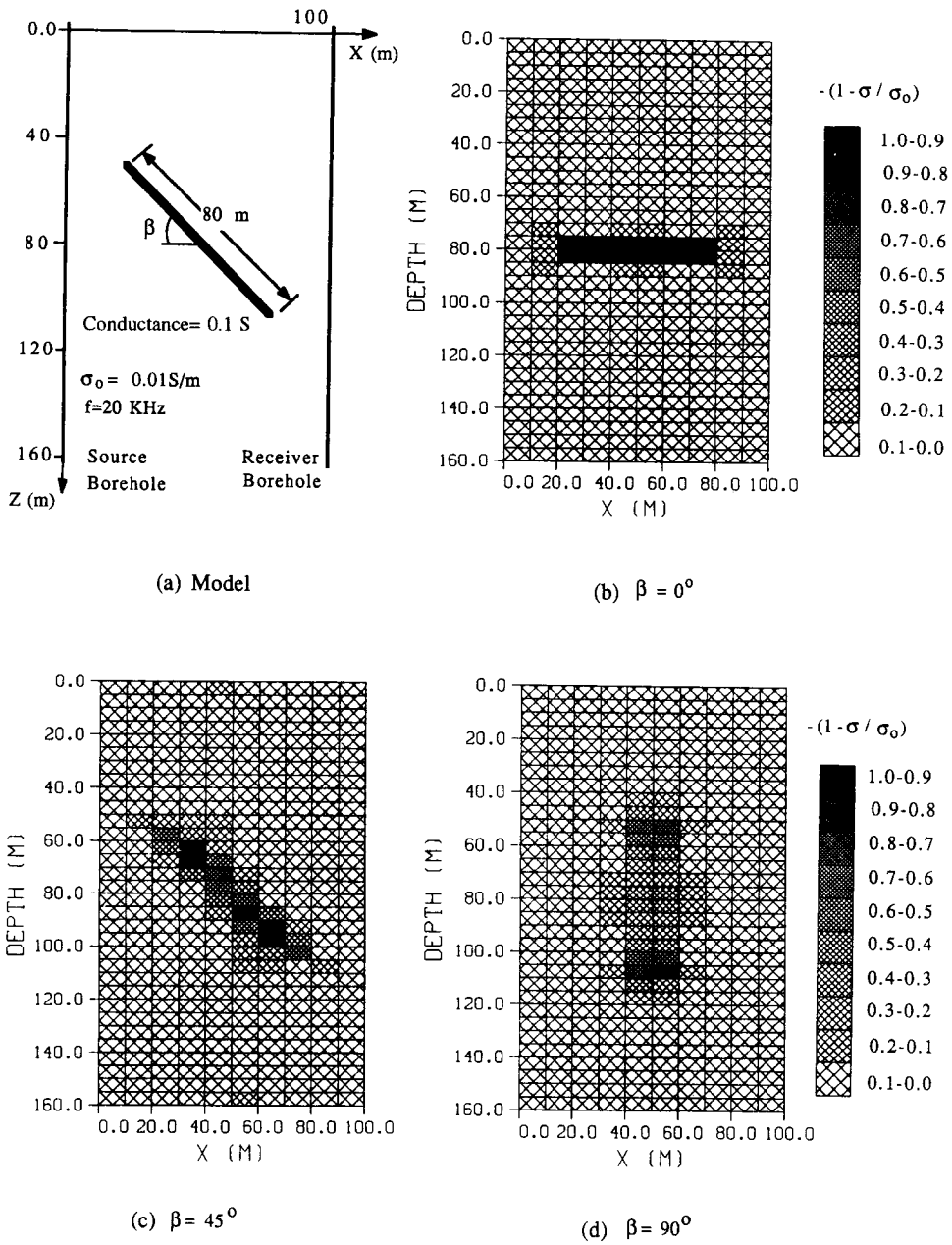

FIG. 6. Images of a thin conductor with different dip angles. (a) Model, (b) $\beta = 0°$, (c) $\beta = 45°$, (d) $\beta = 90°$.

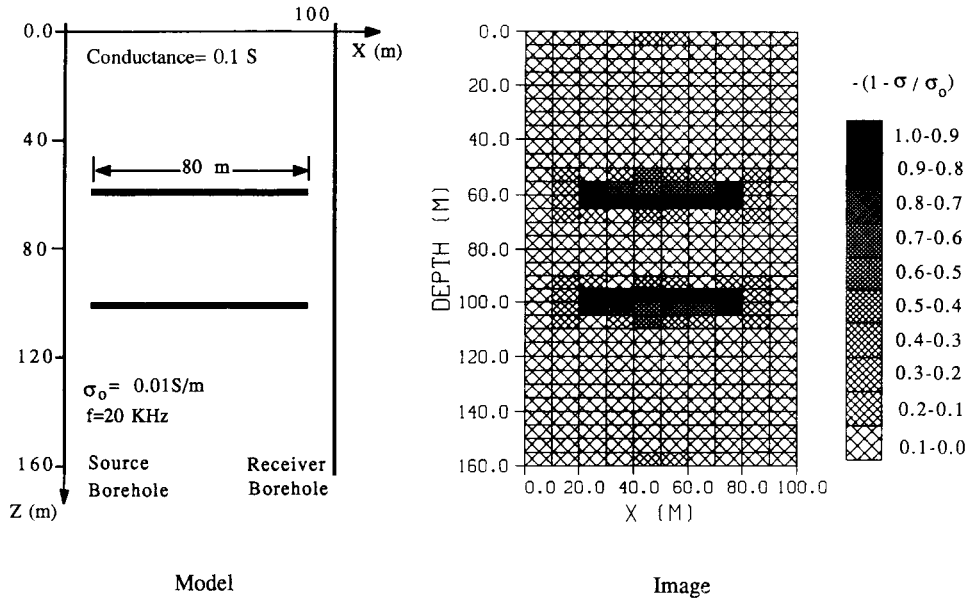

(a) $\beta = 0^o$

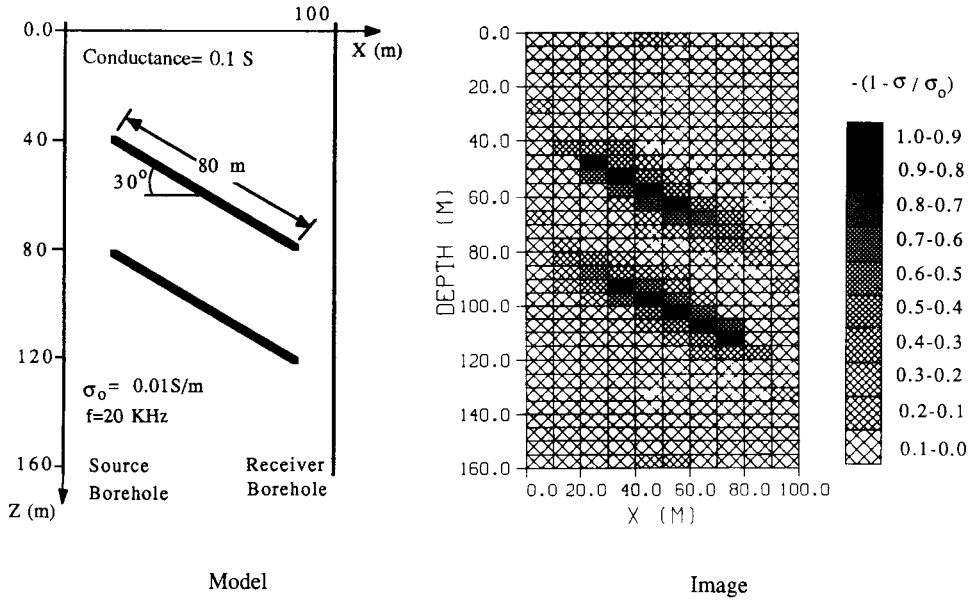

(b) $\beta = 30^o$

FIG. 7. Images of two parallel thin conductors with different dip angles. (a) $\beta = 0°$, (b) $\beta = 30°$, (c) $\beta = 60°$, (d) $\beta = 90°$.

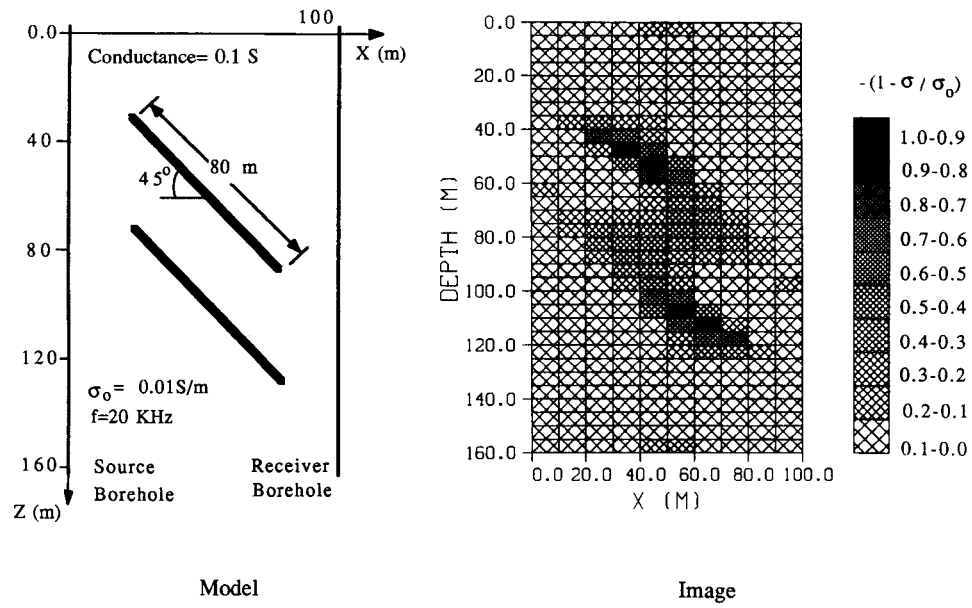

(c) $\beta = 45^{o}$

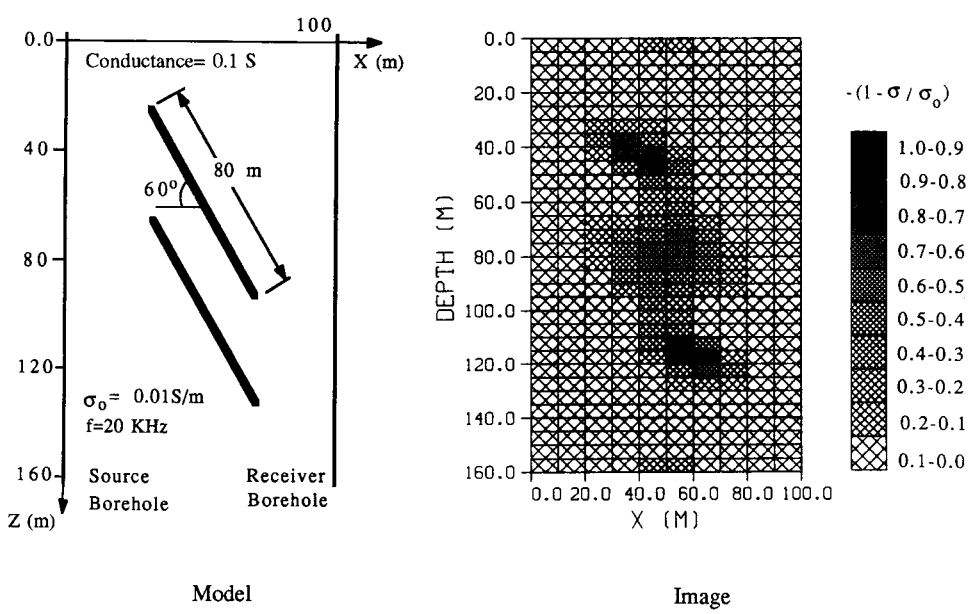

(d) $\beta = 90^{o}$

FIG. 7 Continued

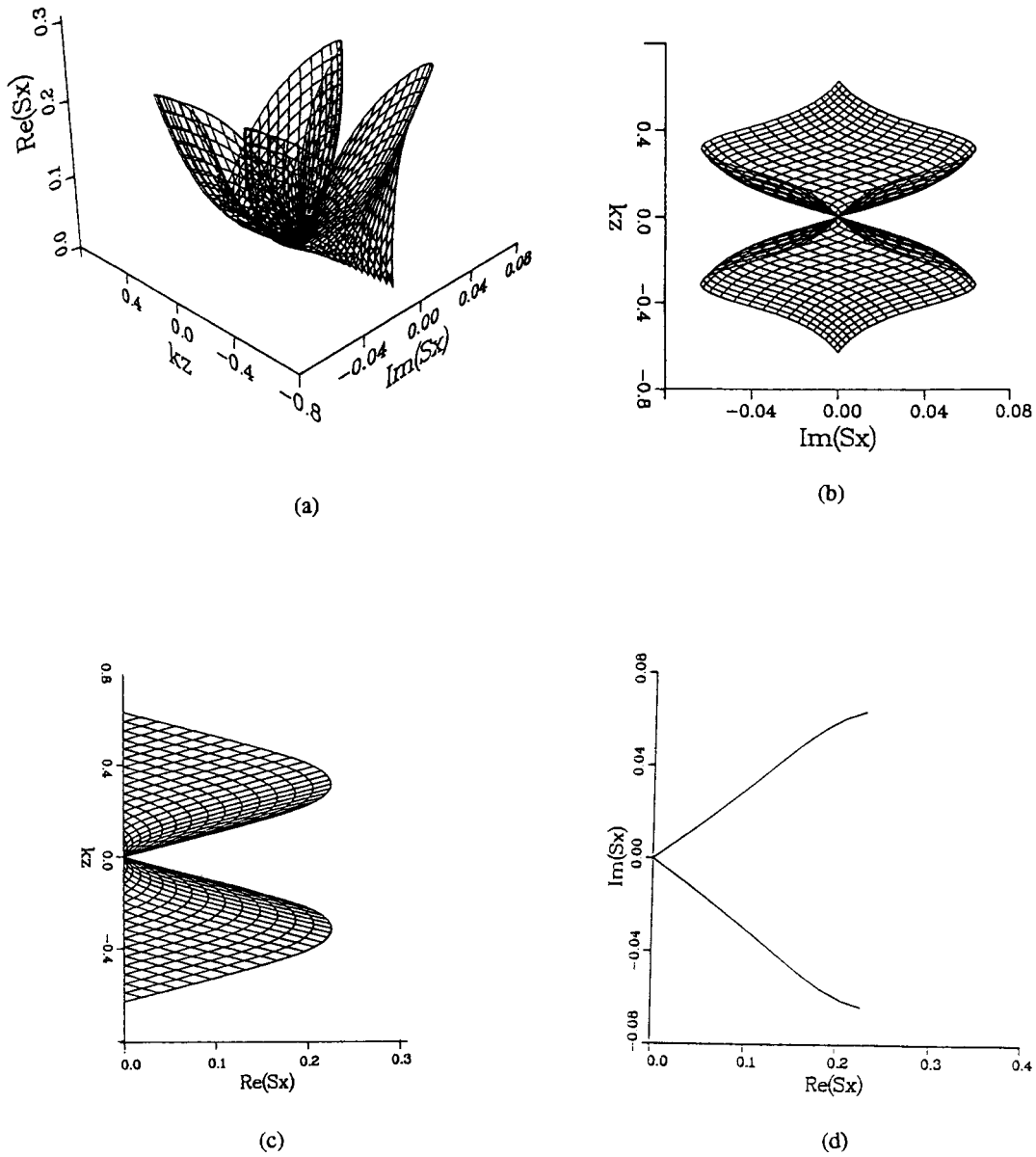

FIG. 8. Wavenumber domain coverage of crosshole transmitter-receiver configuration. (a) k_z versus $Im(s_x)$ and $Re(s_x)$. (b) Projection on the k_z-$Im(S_x)$ plane. (c) Projection on the k_z-$Re(S_x)$ plane. (d) $Im(S_x)$ versus $Re(S_x)$ for $k_z = \pi/\Delta_s$.

the dip angle of a thin conductor or the separation of two point targets are properly recovered since the distortion due to the incomplete coverage (missing high wavenumbers) blurs the image but does not affect the position or orientation.

ACKNOWLEDGMENTS

We wish to express our thanks to Dr. K. H. Lee of Lawrence Berkeley Laboratory and Dr. A. Tura for helpful discussions during the work. Financial support for this work is provided by the U.S. Department of Energy under Contract No. DE-AC03-76SF00098.

REFERENCES

Bracewell, R. N., 1956, Strip integration in radio astronomy: Aust. J. Phys., **9**, 198–217.

Bertero, M., 1982, On the recovery and resolution of exponential relaxation rates from experimental data—Value analysis of the Laplace transform inversion in the presence of noise: Proc. Roy. Soc. Lond., **A383**, 15–29.

Bertero, M., Brianzi, P., and Pike, E. R., 1983, Singular value decomposition of the Laplace transform inversion with discrete data: Series title: Pubblicazioni dell'Istituto di analisi globale e applicazioni. Serie "Problemi non ben posti ed inversi"; No. 1.

Cheng, G., 1984, Exact and approximate solutions to some geophysical inverse problems: Ph.D. thesis, University of California at Berkeley.

Deadrick, F. J., Ramirez, A. L., and Lytle, R. J., 1982, In-situ

fracture mapping using geotomography and brine tracers: IEEE Trans. on Nuclear Science, **NS-29**, No. 1.

Devaney, A. J., 1981, Inverse-scattering theory within the Rytov approximation: Optics Letters, **6**, 374–376.

——— 1984, Geophysical diffraction tomography: IEEE Trans. on geoscience and remote sensing, **GE-22**, No. 1.3-13.

Gill, P. E., Murray, W., and Wright, M. H., 1981, Practical optimization: Academic Press, London.

Gradshteyn, I. S., Ryzhik, I. M., 1980, Table of integrals, series, and products: Academic Press Inc.

Hopper, M. J., 1979, HARWELL subroutine library—A catalog of subroutines: AERE, Harwell, Didcot, Oxon, OX11 ORA, England.

Howard, A. Q., Glass, C. E., Henry, D. B., N'Guessan, D. M., and Siemers, D. M., 1983, Indirect rock mass investigations for optimizing borehole drilling programs, Vol. 4, Wave diffusion geotomography: Univ. of Arizona, Tucson, NUREG/CR-3143-V4.

Huesman, R. H., Gullberg, G. T., Greenberg, W. L., and Budinger, T. F., 1977, Users manual: Donner algorithms for reconstruction tomography: Lawrence Berkeley Laboratory, University of California, Report PUB-214, 285 p.

Kak, A. C., and Slaney, M., 1987, Principles of computerized tomographic imaging: IEEE Press.

Mersereau, R. M., and Oppenheim, A., 1974, Digital reconstruction of multidimensional signals from their projections: Proc. of IEEE, **62**, 1319–1338.

Oristaglio, M. L., 1985, Accuracy of the Born and Rytov approximations for reflection and refraction at a plane interface: J. Optical Soc. Am., 1987–1993.

Pan, S. X., and Kak, A. C., 1983, A computational study of reconstruction algorithms for diffraction tomography: Interpolation versus filtered back propagation: Trans. Acoust. Speech and Signal Proc., IEEE ASSP-31, 1262–1275.

Peterson, J. E., 1986, The application of algebraic reconstruction techniques to geophysical problems: Ph.D. thesis, University of California.

Slaney, M., and Kak, A. C., 1985, Imaging with diffraction tomography: School of Elec. Eng., Purdue University, Report TR-EE 85-5.

Stark, Philip B., 1987, Strict bounds and applications: Proc. of RCP 264 Recontre Interdisciplinaire Problemes Inverses Montpellier, France.

Ward, S., and Hohmann, G. W., 1988, Electromagnetic theory for geophysical applications, *in* Nabighian, M. N., Ed., Electromagnetic methods in applied geophysics—Theory: Investigations in geophysics No. 3, Soc. Expl. Geophys.

Wolf, E., 1969, Three-dimensional structure determination of semi-transparent objects from holographic data: Optics Communications, **1**, 153–156.

Wu, R. S., and Toksöz, M. N., 1987, Diffraction tomography and multisource holography applied to seismic imaging: Geophysics, **52**, 11–25.

Wu, R. S., and Xu, S. H., 1979, Digital holography applied to borehole electromagnetic wave exploration: ACTA Seismologica Sinica, **1**, 197–213.
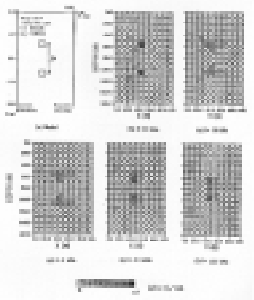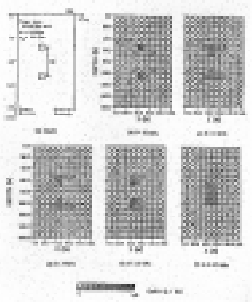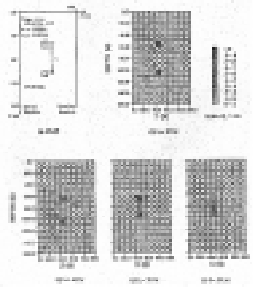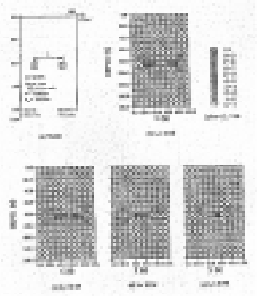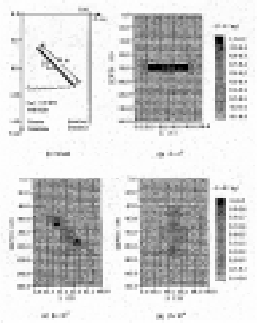
Zhou, Q., 1989, Audio-frequency electromagnetic tomography for reservoir evaluation: Ph.D. thesis, University of California, Berkeley.